

In situ visualization of loading-dependent water effects in a stable metal-organic framework

Nicholas C. Burtch 1,5, Ian M. Walton, Julian T. Hungerford, Cody R. Morelock, Yang Jiao 1, Jurn Heinen, Yu-Sheng Chen, Andrey A. Yakovenko, Wenqian Xu, David Dubbeldam 2 and Krista S. Walton 1,*

Competitive water adsorption can have a significant impact on metal-organic framework performance properties, ranging from occupying active sites in catalytic reactions to co-adsorbing at the most favourable adsorption sites in gas separation and storage applications. In this study, we investigate, for a metal-organic framework that is stable after moisture exposure, what are the reversible, loading-dependent structural changes that occur during water adsorption. Herein, a combination of in situ synchrotron powder and single-crystal diffraction, infrared spectroscopy and molecular modelling analysis was used to understand the important role of loading-dependent water effects in a water stable metal-organic framework. Through this analysis, insights into changes in crystallographic lattice parameters, water siting information and water-induced defect structure as a response to water loading were obtained. This work shows that, even in stable metal-organic frameworks that maintain their porosity and crystallinity after moisture exposure, important molecular-level structural changes can still occur during water adsorption due to guest-host interactions such as water-induced bond rearrangements.

etal-organic frameworks (MOFs) are a class of crystalline, nanoporous materials formed by the assembly of inorganic nodes and multitopic organic linkers¹. Their exceptionally high porosity and tunable structural properties make these materials promising platforms for technologies ranging from gas separation and storage to catalysis, chemical sensing and drug delivery²⁻⁴. A greater understanding of the chemical stability and guest-host interactions of MOFs under practical operating conditions is essential to the design and development of these materials for a variety of applications.

Water is ubiquitous both in the environment and in various industrial streams of many gas separation and purification systems. Due to its highly directional hydrogen bonding behaviour, water exhibits an array of anomalous behaviours, such as increased density upon melting, a density maximum as a normal liquid at 4 °C and decreasing viscosity with increasing pressure⁵. The dipole moment, hydrogen bonding properties and nucleophilic character of water can lead to a variety of guest–host interactions within a MOF lattice. For application purposes, it is therefore critically important to understand the impact of water on the stability and adsorptive performance properties of MOFs⁶.

While a number of MOFs undergo degradation in the presence of water vapour, the list of frameworks that display a high degree of water stability is quickly growing⁷⁻⁹. Among these frameworks, a limited number of MOFs exhibit large-scale structural transitions in humid environments¹⁰⁻¹². However, outside of this subset of frameworks, the impact of water interactions on the structural properties of stable MOFs remains largely unknown. In particular, given the crucial role defects can have in dictating framework stability and performance properties, understanding defect structure and formation has become a topic of growing importance in the MOF

community^{13–16}. Defect formation is traditionally thought to occur during MOF assembly or to arise from post-synthetic modification of the framework¹⁵. A greater understanding into the guest–host interactions within MOFs that give rise to defect formation during adsorption processes, however, is another critical aspect of this field.

In this work, we present crystallographic evidence of the importance of loading-dependent water effects on the structural properties of a water stable MOF that does not undergo large-scale structural transitions upon interactions with water. Our findings are consistent with a scenario where bond rearrangement occurs in the presence of water, but does not result in irreversible structural changes or degradation. We demonstrate these effects via a series of in situ synchrotron X-ray diffraction (XRD) experiments, infrared (IR) spectroscopy and molecular simulation analysis on the DMOF-TM framework, $Zn_2(BDC-TM)_2(DABCO)$ (BDC-TM = 2,3,5,6-tetramethyl-1,4-benzenedicarboxylic acid, DABCO = 1,4-diazabicyclo[2.2.2]octane)¹⁷ (Fig. 1a). This framework is an isostructural variant of the prototypical DMOF-1 framework¹⁸ with superior water stability and low-pressure CO₂ affinity properties due to the presence of methyl groups on the terephthalate ligand¹⁹. The methyl functional groups do not prevent water from entering the pore space but nonetheless play a critical role in improving the material's moisture stability^{20,21}. The exact origin of the increased stability is not fully understood; however, this understanding has important broader implications given the emerging crystal engineering strategy of using linker design for improving MOF chemical stability and functionality properties^{6,22}. The stability of DMOF-TM, combined with the ability to reversibly adsorb significant amounts of water, also makes it an attractive candidate for understanding the loadingdependent structural changes that occur during water adsorption in a stable MOF.

¹School of Chemical and Biomolecular Engineering, Georgia Institute of Technology, Atlanta, GA, USA. ²Van't Hoff Institute for Molecular Sciences, University of Amsterdam, Amsterdam, The Netherlands. ³ChemMatCARS, University of Chicago, Argonne, IL, USA. ⁴X-ray Science Division, Advanced Photon Source, Argonne National Laboratory, Argonne, IL, USA. ⁵These authors contributed equally: Nicholas C. Burtch, Ian M. Walton. *e-mail: krista.walton@chbe.gatech.edu

ARTICLES NATURE CHEMISTRY

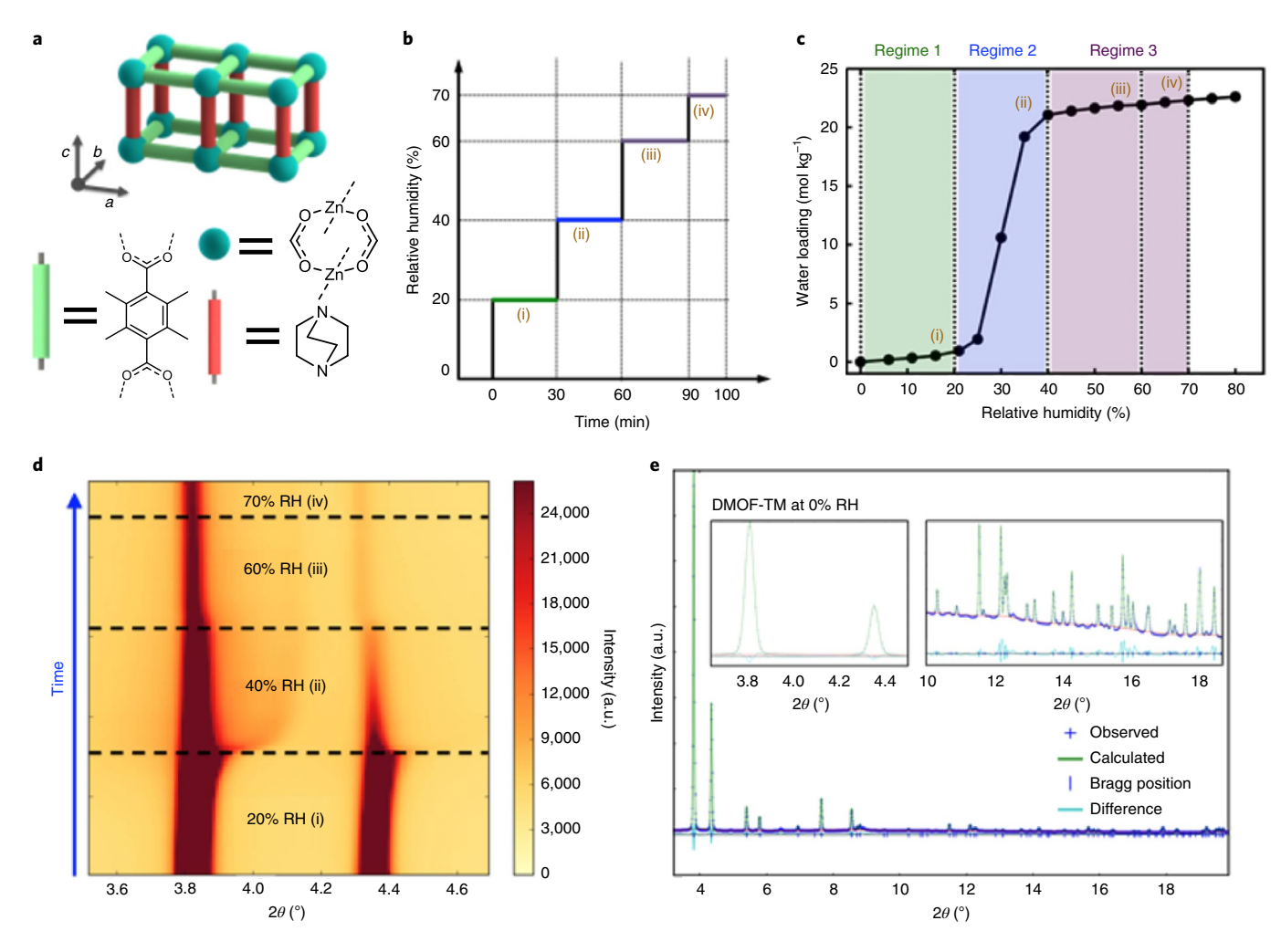


Fig. 1 | Insitu synchrotron powder diffraction experiments. **a**, Structure and schematic representation of the DMOF-TM framework, Zn₂(BDC-TM)₂(DABCO) and related molecular building blocks: the Zn paddlewheel cluster (dark green) and the two linkers, **BDC-TM** (light green) and **DABCO** (red). **b**, Humidity exposure conditions as a function of time throughout the in situ powder diffraction experiment. **c**, Equilibrium water loadings in DMOF-TM under different humidity conditions at 298 K, with points (i)–(iv) indicating the equilibrium water loadings expected under the in situ exposure conditions shown in **b**. **d**, Evolution of the (110) and (001) Bragg peaks for DMOF-TM with moisture exposure and time (λ = 0.72768 Å). **e**, Rietveld fit for the *P4/nbm* space group DMOF-TM structure with selected low and high 2θ regions magnified (insets).

Results and discussion

Synthesis and characterization. DMOF-TM samples were synthesized through the reaction of zinc nitrate hexahydrate, BDC-TM and **DABCO** in N,N'-dimethylformamide (DMF) using a solvothermal synthesis procedure²⁰. Ensuring the sample contains microcrystalline powder with random crystallite orientations is essential for good counting statistics during powder diffraction analysis²³. To facilitate this, the sample was immersed in methanol and lightly ground prior to synchrotron powder diffraction experiments. Nitrogen and water physisorption analyses before and after mechanical grinding of the sample were also performed to ensure retention of porosity characteristics after grinding (Supplementary Figs. 3 and 5). DMOF-TM crystals suitable for single-crystal analysis were grown through a similar solvothermal reaction. However, hydrochloric acid was added to inhibit the immediate reaction of linker and zinc atoms, and a lower temperature was used to slow crystal growth. Further details on the sample synthesis, preparation and characterization procedures are provided in the Methods and Supplementary information sections.

In situ powder diffraction. Residual methanol was first removed from the DMOF-TM sample in situ at the beamline under helium at

250 °C, based on thermogravimetric analysis results. After cooling to room temperature, the relative humidity (RH) of the sample environment was varied in a step-wise fashion (Fig. 1b), and high-resolution diffraction patterns were collected at one-minute intervals.

To understand the structure's water affinity, separate adsorption experiments were performed on an analogously ground DMOF-TM sample to determine the equilibrium water loading over the 0–70% RH range (Fig. 1c). The points labelled (i)–(iv) on Fig. 1c correspond to the framework's equilibrium water loading at the corresponding conditions given in Fig. 1b. Based on Fig. 1c, the water adsorption behaviour of DMOF-TM during the synchrotron experiments can be divided into three regimes: (1) regime 1, corresponding to 20% RH, where relatively low water loadings are present in the structure, (2) regime 2, corresponding to 40% RH, where significant water adsorption is occurring and (3) regime 3, corresponding to 60% and 70% RH, where the loadings have approached saturation and only incremental amounts of water are being adsorbed.

Knowing the framework's water affinity, structural changes during the in situ powder diffraction experiments were then correlated with the water loading. The contour plot in Fig. 1d shows how the (110) and (001) Bragg peaks (near 3.8° and 4.4° in 2θ , respectively) evolve throughout the three different adsorption regimes. Before moisture

NATURE CHEMISTRY ARTICLES

was introduced into the system, the Rietveld refinement agreement shown in Fig. 1e for DMOF-TM was obtained using the single-crystal XRD (SCXRD) model derived from experiments described later in the text. Upon initial moisture exposure (regime 1), changes to the diffraction pattern were minor and manifest as peak broadening, a phenomenon that is attributed to increased crystal microstrain caused by the formation and presence of defects^{23,24}. At the onset of significant water adsorption (regime 2), a broad shoulder indicative of amorphous character appears near the (110) peak, and the relative intensity of the (001) peak decreases significantly due to water effects. As the water loading approaches saturation (regime 3), the (001) peak undergoes a noticeable shift to lower 2θ values and further indicates a reduction in intensity. As discussed below, these water-induced structural changes are reversible and have origins that are more complex than the well-studied contraction and swelling behaviours found in other nanoporous materials²⁵.

Evolution of crystallographic lattice parameters. To quantitatively understand the water-induced structural response, lattice parameters were determined (Fig. 2a) via Pawley refinement²⁶ of the in situ powder diffraction data using the tetragonal (*P4/nbm*) DMOF-TM structure obtained in the synchrotron SCXRD experiments (Supplementary Table 2). Rietveld refinement²⁷ of regime 1 data yielded lattice parameters that are consistent with the Pawley refinement results. However, Rietveld refinement of regime 2 and 3 data was complicated by the changes to peak shapes that were attributed to high water loadings in the framework.

In regime 1, the lattice volume undergoes a contraction, which was attributed to initial water-induced defect formation. The structural changes noted in regime 2 were attributed to significant water adsorption, resulting in the formation of water clusters that occupy the pore space and serve to compensate for the defect-induced contraction of regime 1. Finally, as pore saturation is reached in regime 3, there is a large increase in the lattice volume for each incremental amount of water adsorbed. Insights into the chemical physics of the framework during the adsorption process, as well as characterization of the structural changes and proposed water-induced defects, were obtained via in situ SCXRD, in situ IR spectroscopy and molecular simulation analysis.

Structural changes. Using the equilibrium water loadings given in Fig. 1c, molecular modelling studies were performed to explore the proposed structural changes of Fig. 2b. A similar low loading contraction behaviour to that observed in regime 1 has been found in other nanoporous materials and has been attributed to a straininduced deformation mechanism upon adsorption²⁸. In high-pressure diffraction experiments, lattice compression can occur prior to expansion due to external pressure acting on the sample^{29,30}. We propose that the water-induced contraction behaviour observed in DMOF-TM can be attributed to distinct effects. First, for a straininduced contraction, classical simulations using a flexible framework model should capture such contractions at low water loadings. No evidence of such contractions was observed in the simulations (Supplementary Fig. 25), and instead a minor increase in the lattice volume at low water loadings was noted. Furthermore, analysis of in situ IR spectroscopy experiments under similar loading conditions suggests water-induced interactions consistent with a change in carboxylate environment and possible binding mode with the paddle wheel (Supplementary Fig. 10). These observations are also in line with those reported in past IR spectroscopy experiments with D₂O as a probe molecule, where water-induced changes assigned to deuterium bonding interactions between water and the framework carbonyl groups and interactions involving adjacent carbonyl groups were observed³¹.

In regimes 2 and 3, Fig. 1c indicates that pore filling followed by pore saturation occurs. In situ IR spectroscopy experiments

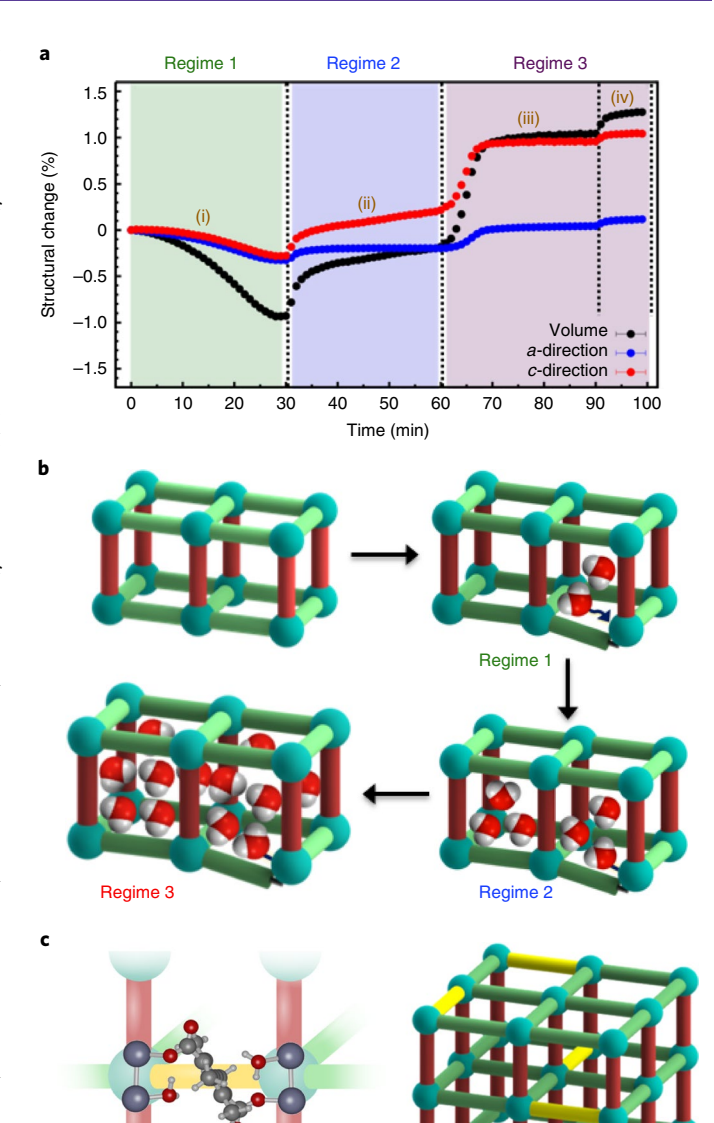


Fig. 2 | Water-induced structural changes. a, Evolution of crystallographic structural parameters as a function of time and moisture content from in situ powder diffraction experiments. **b**, Schematic of the water-loading process's impact on the experimental crystallographic parameters and structure, as evidenced from XRD and IR experiments. **c**, Depiction of a proposed defect scenario consistent with SCXRD and IR spectroscopy data where unidentate carboxylate defects are generated from the insertion of water molecules in a *cis* fashion at opposite paddle-wheel sites (shown in yellow). Colour code as per Fig. 1; for the water molecules and defect shown in **c**: C, dark grey; O, red; H, light grey.

indicate that the changes in carboxylate environment persisted in these regimes. However, the relatively large lattice expansion observed in regime 3 was attributed, based on the flexible framework simulations of Supplementary Fig. 25, to the adsorptive stress exerted on the pore walls at these water loadings. At low water loading, simulations suggest that water is primarily located near the carboxylate oxygen atoms and, as pore filling occurs, the favoured adsorption sites shift towards the centre of the pore (Supplementary Fig. 28). The large increase in lattice volume for each additional water molecule adsorbed near pore saturation is attributed to the higher degree

ARTICLES NATURE CHEMISTRY

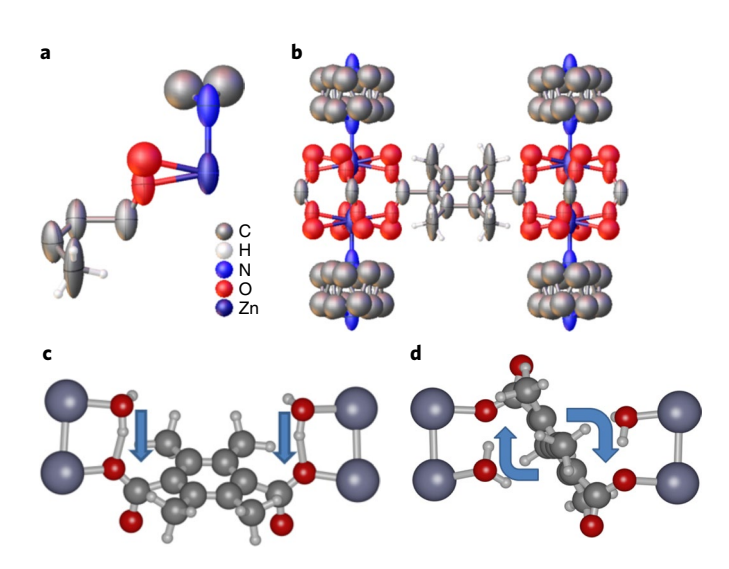


Fig. 3 | Defect structures. a, Asymmetric unit of the SCXRD structure of the defective DMOF-TM. Partial occupancy of water-induced defects above the carboxylate oxygen. **b**, Expanded asymmetric unit detailing a single **BDC-TM** linker, two Zn paddle wheels and four pillaring **DABCO** linkers. Defect oxygen atoms are present at all sites by symmetry. **c,d**, Proposed *cis* (**c**) and *trans* (**d**) defect structures. As indicated by the arrows, quantum mechanical calculations (Supplementary information, theoretical defects calculations) support the *cis* defect structure forming due to a water-induced translation of the linker, whereas the *trans* defect structure originates from a water-induced linker rotation.

of intermolecular repulsion that each of these molecules experience. Because of this, relative to the previously adsorbed molecules, each additional water molecule in regime 3 provides a larger contribution to the strain-induced expansion of the framework.

To better understand the structure of the water-induced defects, a series of SCXRD studies were performed. All structures obtained from SCXRD experiments were found to index to a different unit cell than the previously reported DMOF-TM structure and to have the *P4/nbm* space group¹⁷. In addition to standard data collections, dynamic in situ SCXRD experiments were carried out to investigate the structural response of DMOF-TM to varied relative humidity environments (see Supplemental information, in situ synchrotron SCXRD)^{32,33}.

In all SCXRD structures, electron density proximal to the terephthalate linker oxygen was observed and modelled to a partial occupancy oxygen atom (Fig. 3a). The partial occupancy (defect) oxygen atoms were used to quantify the number of water-induced defects formed in the DMOF-TM crystal. Theoretical calculations were also performed to examine the possible causes of the defects and the impact of water adsorption on the structure (see Supplemental information, theoretical defect calculations). The defect oxygen occupancy remained relatively constant between 15 and 25% at various relative humidity levels (see Supplemental information, in situ synchrotron SCXRD). Preparation of the crystals for dynamic in situ SCXRD data collections resulted in the activation and exposure of the samples to ambient humidity, which precluded data collection on an activated structure similar to the reference structure of Fig. 2a, which underwent heat pretreatment. However, in situ powder XRD and IR experiments indicated a reversion of the water-induced defects on application of heat in a dry environment (details in Supplemental information, in situ synchrotron powder diffraction and laboratory characterization, respectively).

Understanding the structure of the defect (substitutional disorder) in the framework was complicated by the high symmetry of the linker and the framework; given the position of the defect in the asymmetric unit, the defect had a statistical chance of occurring at each terephthalate oxygen (Fig. 3b). Determining the structural change in the framework to accommodate the water-induced defect therefore required complimentary in situ IR experiments and computations. Three potential structural rearrangements to accommodate water insertion at the zinc paddle wheel were considered, each consisting of a combination of linker translation and carboxylate rearrangement. All proposed defect scenarios consisted of two defect sites at a single linker, thus requiring partial displacement of the linker to accommodate the inserted oxygen atoms. Two of the proposed defect structures involved the insertion of water molecules at the associated paddle-wheel modes with a cis or trans insertion profile with respect to the linker, with a corresponding change in the bridging carboxylate binding groups from bidentate to unidentate to accommodate the water insertion while maintaining the connectivity of the framework (Fig. 3c,d). The third defect scenario consisted of the formation of a dangling linker defect, in which a water and a hydroxyl group replace the carboxylate linkage at the paddle wheel (Supplementary Fig. 22). The dangling linker defect was found to be disfavoured by the in situ IR experiments, as shown by the lack of a peak characteristic of a carboxylic acid carbonyl group (Supplementary Fig. 10). The cis and trans defect structures were further analysed via quantum mechanical calculations in the Supplemental information. All anisotropically refined atoms displayed positional disorder approximately aligned with the c-axis, consistent with the translation of the linker in the proposed cis and trans defect structures. In all SCXRD structures, the ligand-metal-ligand (DABCO-zinc-defect) angle was found to be between 75° and 85°. This deviation from the ideal 90° of an octahedral metal complex indicates a steric interaction between the defect and the displaced linker. Should the linker be completely displaced, a 90° angle would be expected. Last, theoretical calculations indicate that the orientation of the BDC-TM ligand enables highly favourable water hydrogen bonding interactions that are not possible in the less stable DMOF-1 framework (Supplementary Fig. 41). These more favourable adsorption interactions, in concert with the proposed structural rearrangements, may explain the greater stability of DMOF-TM relative to DMOF-1 as they stabilize the DMOF-TM reactant state before further bond breakage can occur.

The overall reversibility of the water adsorption process is also supported by additional adsorption and desorption isotherms measured as a function of temperature (Supplementary Fig. 6). Furthermore, negligible changes in porosity characteristics are evidenced from N_2 physisorption measurements at 77 K, with the reversibility of the IR spectroscopy data also indicating that the water-induced defects are removed upon heating (Supplementary Fig. 11)³¹. No IR spectroscopy evidence suggests protonation of carboxylic acid groups during water adsorption (Supplementary Fig. 10).

Water siting information. To further understand the behaviour of water within the structure, difference envelope density maps^{34,35} were calculated from the powder diffraction data to visualize the preferred crystallographic sites for water throughout the adsorption process. The analysis, shown in Fig. 4a, can provide insight into scenarios where unwanted water co-adsorption may occur and have a detrimental effect on a material's adsorption properties. At low water loadings, the maximum water density is concentrated between the terephthalate and **DABCO** linkers in the structure. However, as water loading increases, the maximum density region for water spreads away from the linkers and eventually locates in the centre of the pore space under saturation conditions. This scenario, in which water begins near the hydrophilic framework sites before transitioning to the centre of the pore at higher loadings, is also consistent with the molecular modelling behaviour discussed in the preceding section. Further details on the analysis of the difference envelope density are presented in the Supplemental information. Attempts to NATURE CHEMISTRY ARTICLES

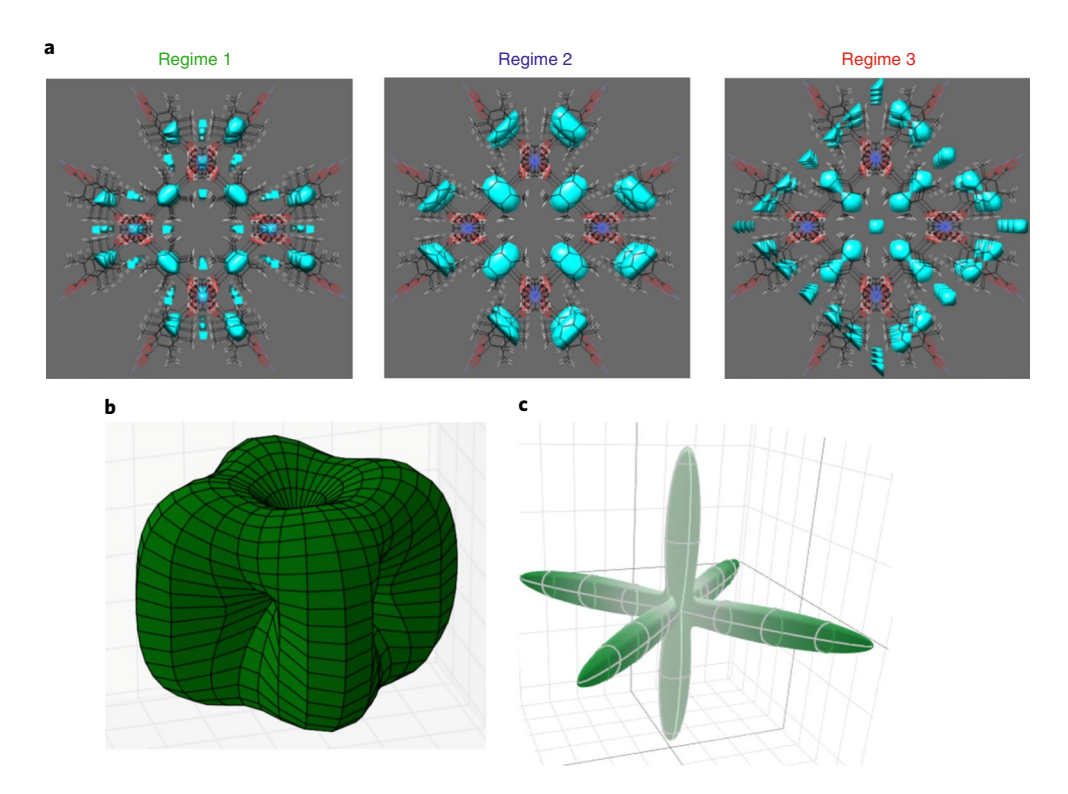


Fig. 4 | Water siting, microstrain and Young's modulus analysis. a, Representative difference envelope density plots generated from the most intense low-index diffraction reflections to show water siting in the crystallographic *c* direction. At low water loadings (regime 1), the maximum water density is between the terephthalate and **DABCO** linkers in the structure and, as water loading increases (regimes 2 and 3), the maximum density spreads away from the linkers and towards the centre of the pore. **b**, Experimental microstrain plot for the evacuated structure, obtained from peak broadening behaviour in the synchrotron powder diffraction data. Microstrain arises from non-uniform lattice distortions that create deviations in *d* spacings in a crystallographic plane. **c**, Calculated Young's modulus for the evacuated structure, derived from an analysis of the elastic constant tensor of a DMOF-TM flexible force field framework model⁴². The inverse correlation between this plot and the experimental microstrain of **b** implies that the refinement of (synchrotron) powder diffraction data may be used as a tool for understanding the Young's modulus of MOFs.

obtain quantitative information regarding water partial occupancies in the structure were also made via Rietveld analysis, although these efforts were unsuccessful due to the high level of disorder present under the room temperature measurement conditions.

Microstrain and Young's modulus analysis. Finally, the sample's microstrain behaviour was analysed to further understand its structural response to water. Microstrain arises from non-uniform lattice distortions that create deviations in *d* spacings in a crystallographic plane, resulting in peak broadening^{23,24}. Accounting for the peak broadening caused by this microstrain produced the experimental microstrain plot for the evacuated structure shown in Fig. 4b. As noted above, at low water loadings the magnitude of microstrain increases, indicating increased defect presence in the structure. Beyond regime 1, peak broadening due to significant water adsorption precluded further interpretation of the microstrain.

By calculating the elastic tensor of the energy-minimized structure using a previously reported DMOF-TM flexible framework model³¹, the theoretical Young's modulus for the evacuated structure was produced (Fig. 4c). Maxima in the experimental microstrain correspond to directions of greatest strain whereas maxima in the Young's modulus correspond to directions of greatest stiffness. Intuitively, the crystallographic directions corresponding to the ligand anchoring points in the structure are the same directions that exhibit the lowest degree of experimental microstrain. The inverse correlation between our experimental microstrain and the calculated Young's modulus implies that the refinement of (synchrotron) powder diffraction data may be used to understand the Young's modulus of certain MOFs. The experimental Young's modulus of frameworks is usually obtained

from nanoindentation experiments, for which limited experiments have been performed³⁶; this analysis suggests that similar information related to MOF mechanical properties, which can have important implications for understanding their utility for technological applications³⁷, may be extracted from a simpler analysis of the microstrain behaviour from powder diffraction data.

Conclusions

These findings highlight the reality that, even for MOFs that are highly stable in humid environments, a static representation of the framework structure may not be sufficient to understand the observed stability. This work has shown that the DMOF-TM framework has a dynamic and reversible structural response to water guest molecules, observed in changes in the unit cell parameters, microstrain, vibrational spectra and atomic structure. These changes manifest themselves at low guest loading and continue to change in response to guest loading. This study illustrates the importance and complexity of guest-host interactions on the stability of MOFs. Further, the dynamic structural response of the DMOF-TM framework to guest water molecules reveals the importance of studying structures without large-scale structural transitions in greater detail. In future work, valuable insight may be obtained from metadynamics³⁸ or transition path sampling techniques that can efficiently sample the coordination of water in the framework and its respective energy barrier. While the ligand functionality and coordination environment found in this framework are not representative of a number of MOFs reported in the literature, this work nonetheless furthers our understanding of the array of factors that must be considered in understanding MOF performance and stability properties.

ARTICLES NATURE CHEMISTRY

Methods

Sample synthesis and preparation. Polycrystalline DMOF-TM was synthesized by mixing Zn(NO₃)₂·6H₂O (189 mg), 2,3,5,6-tetramethyl-1,4-benzenedicarboxylic acid (140 mg) and 1,4-diazabicyclo[2.2.2]octane (35 mg) in DMF (15 ml) at room temperature. The mixture was then mixed on a stir plate for two hours before the solution was transferred to a Teflon-lined stainless-steel reactor and placed in a preheated oven at 120 °C for two days. The resulting solution was removed from the oven and allowed to cool to room temperature in air before being filtered and repeatedly washed with DMF. Prior to powder diffraction measurements, the sample was immersed in methanol and lightly ground using a mortar and pestle.

Crystals suitable for SCXRD analysis were grown through a modification of the above synthesis procedure where 2,3,4,5-tetramethylterephthtalic acid (22 mg) and 1,4-diazabicyclo[2.2.2] octane (6 mg) were dissolved in DMF (20 ml). The solution was briefly sonicated to ensure all reagents went into solution. To the solution, HCl (8 μ l) was added. Following the addition of Zn(NO₃)₂•6H₂O (30 mg), the solution was split into two separate 15 ml thick-walled glass pressure vessels. The vessels were sealed and heated to 100 °C for three days. The reaction was allowed to cool to room temperature slowly. The recovered plate crystals were washed with fresh DMF, then solvent exchanged with CHCl₃ for at least four days prior to data collection.

Synchrotron experiments. In situ powder diffraction experiments were performed at beamline 17-BM-B of the Advanced Photon Source at Argonne National Laboratory with X-rays of $\lambda = 0.72768$ Å. The relative humidity of the sample environment was controlled within a previously described flow cell set up by varying the ratio of mass flow rates of a humidified and dry helium stream at a total flow rate of 30 cc min⁻¹. The GSAS-II software was used to perform all Pawley²⁶ and Rietveld²⁷ refinement analyses on the powder diffraction data.

In situ SCXRD experiments were performed at the ChemMatCars beamline (15-IDD) of the Advanced Photon Source at Argonne National Laboratory. All data were collected on a Pilatus 3X CdTe 1M detector with λ =0.41328 Å radiation at room temperature (293 K). Further details on data collection strategies for dynamic in situ and static data collection can be found in the Supplemental information.

Molecular simulation methodology. Classical simulations employed the RASPA molecular simulation software for adsorption and diffusion in flexible nanoporous materials⁴¹ using a DMOF-TM flexible force field model parameterized in previous work⁴². The Young's modulus for the evacuated structure was derived from the elastic tensor of the energy-minimized framework model and plotted using the ELATE tool⁴³. Periodic density functional theory calculations were performed using the VASP package⁴⁴. Some images were created with CrystalMaker, a crystal and molecular structures programme for Mac and Windows (CrystalMaker Software).

Data availability

Data supporting the claims and findings of this paper are available within the Supplementary Information or are available upon request from the corresponding author. Crystallographic data for all structures reported in this paper have been deposited with the Cambridge Crystallographic Data Centre (CCDC), CCDC numbers 1864840 (DMOF-TM_crystal 09_Flow_01), 1864836 (DMOF-TM_ crystal 09 Flow 02), 1864833 (DMOF-TM crystal 09 Flow 03), 1864842 (DMOF-TM_crystal 09_Flow_04), 1864834 (DMOF-TM_crystal 09_Flow_05), 1864835 (DMOF-TM_crystal 09_Flow_06), 1864838 (DMOF-TM_crystal 09_Flow_07), 1864837 (DMOF-TM_crystal 09_Flow_08), 1864839 (DMOF-TM_ crystal 09, static) and 1864841 (DMOF-1, crystal 15, static; where crystal 09 and crystal 15 were both selected from the same batch). Copies of the crystallographic data can be obtained at https://www.ccdc.cam.ac.uk/structures/ free of charge. A SCXRD structure of the 'activated' DMOF-TM structure could not be obtained; unit cell parameters and atomic positions were obtained by Rietveld refinement, refined to the SCXRD data from this study (P4/nbm) and also to the structure previously reported for this material (P4/mmm).

Online content

Any Nature Research reporting summaries, source data, extended data, supplementary information, acknowledgements, peer review information; details of author contributions and competing interests; and statements of data and code availability are available at https://doi.org/10.1038/s41557-019-0374-y.

Received: 16 January 2017; Accepted: 11 October 2019; Published online: 02 December 2019

References

- Zhou, H.-C., Long, J. R. & Yaghi, O. M. Introduction to metal-organic frameworks. Chem. Rev. 112, 673-674 (2012).
- Furukawa, H., Cordova, K. E., O'Keeffe, M. & Yaghi, O. M. The chemistry and applications of metal-organic frameworks. Science 341, 1230444 (2013).

- Kreno, L. E. et al. Metal-organic framework materials as chemical sensors. Chem. Rev. 112, 1105–1125 (2012).
- Stassen, I. et al. An updated roadmap for the integration of metal-organic frameworks with electronic devices and chemical sensors. *Chem. Soc. Rev.* 46, 3185–3241 (2017).
- Nilsson, A. & Pettersson, L. G. M. The structural origin of anomalous properties of liquid water. *Nat. Commun.* 6, 8998 (2015).
- Burtch, N. C., Jasuja, H. & Walton, K. S. Water stability and adsorption in metal-organic frameworks. Chem. Rev. 114, 10575–10612 (2014).
- Bosch, M., Zhang, M. & Zhou, H. Increasing the stability of metal-organic frameworks. Adv. Chem. 2014, 1–8 (2014).
- 8. Howarth, A. J. et al. Chemical, thermal and mechanical stabilities of metal-organic frameworks. *Nat. Rev. Mater.* 1, 15018 (2016).
- Canivet, J., Fateeva, A., Guo, Y., Coasne, B. & Farrusseng, D. Water adsorption in MOFs: fundamentals and applications. *Chem. Soc. Rev.* 43, 5594–5617 (2014).
- Horike, S., Shimomura, S. & Kitagawa, S. Soft porous crystals. *Nat. Chem.* 1, 695–704 (2009).
- Schneemann, A. et al. Flexible metal-organic frameworks. Chem. Soc. Rev. 43, 6062–6096 (2014).
- 12. Zeng, M. H. et al. Apical ligand substitution, shape recognition, vapor-adsorption phenomenon, and microcalorimetry for a pillared bilayer porous framework that shrinks or expands in crystal-to-crystal manners upon change in the cobalt(II) coordination environment. *Inorg. Chem.* 48, 7070–7079 (2009).
- Bennett, T. D., Cheetham, A. K., Fuchs, A. H. & Coudert, F.-X. Interplay between defects, disorder and flexibility in metal-organic frameworks. *Nat. Chem.* 9, 11–16 (2017).
- Sholl, D. S. & Lively, R. P. Defects in metal-organic frameworks: challenge or opportunity? J. Phys. Chem. Lett. 6, 3437–3444 (2015).
- Fang, Z., Bueken, B., De Vos, D. E. & Fischer, R. A. Defect-engineered metal-organic frameworks. Angew. Chem. Int. Ed. 54, 7234-7254 (2015).
- Trickett, C. A. et al. Definitive molecular level characterization of defects in UiO-66 crystals. Angew. Chem. Int. Ed. 54, 11162–11167 (2015).
- Chun, H., Dybtsev, D. N., Kim, H. & Kim, K. Synthesis, X-ray crystal structures, and gas sorption properties of pillared square grid nets based on paddle-wheel motifs: implications for hydrogen storage in porous materials. Chem. Eur. J. 11, 3521–3529 (2005).
- Dybtsev, D. N., Chun, H. & Kim, K. Rigid and flexible: a highly porous metal-organic framework with unusual guest-dependent dynamic behavior. *Angew. Chem. Int. Ed.* 43, 5033-5036 (2004).
- Burtch, N. C. & Walton, K. S. Modulating adsorption and stability properties in pillared metal—organic frameworks: a model system for understanding ligand effects. Acc. Chem. Res. 48, 2850–2857 (2015).
- Jasuja, H., Burtch, N. C., Huang, Y., Cai, Y. & Walton, K. S. Kinetic water stability of an isostructural family of zinc-based pillared metal-organic frameworks. *Langmuir* 29, 633–642 (2013).
- Jasuja, H., Jiao, Y., Burtch, N. C., Huang, Y. & Walton, K. S. Synthesis of cobalt-, nickel -, copper -, and zinc-based, water-stable, pillared metal– organic frameworks. *Langmuir* 30, 14300–14307 (2014).
- Lu, W. et al. Tuning the structure and function of metal-organic frameworks via linker design. Chem. Soc. Rev. 43, 5561-5593 (2014).
- Pecharsky, V. K. & Zavalij, P. Y. Fundamentals of Powder Diffraction and Structural Characterization of Materials Vol. 69 (Springer, 2009).
- Mittemeijer, E. J. & Welzel, U. The "state of the art" of the diffraction analysis
 of crystallite size and lattice strain. Z. Kristallogr. 223, 552–560 (2008).
- Gor, G. Y., Huber, P. & Bernstein, N. Adsorption-induced deformation of nanoporous materials—a review. Appl. Phys. Rev. 4, 011303 (2017).
- Pawley, G. S. Unit-cell refinement from powder diffraction scans. J. Appl. Crystallogr. 14, 357–361 (1981).
- Rietveld, H. M. A profile refinement method for nuclear and magnetic structures. J. Appl. Cryst. 2, 65–71 (1969).
- Ravikovitch, P. I. & Neimark, A. V. Density functional theory model of adsorption deformation. *Langmuir* 22, 10864–10868 (2006).
- Moggach, S. A., Bennett, T. D. & Cheetham, A. K. The effect of pressure on ZIF-8: increasing pore size with pressure and the formation of a highpressure phase at 1.47 GPa. Angew. Chem. Int. Ed. 121, 7221–7223 (2009).
- Hobday, C. L. et al. Understanding the adsorption process in ZIF-8 using high pressure crystallography and computational modelling. *Nat. Commun.* 9, 1429 (2018).
- Burtch, N. C. et al. Understanding DABCO nanorotor dynamics in isostructural metal–organic frameworks. J. Phys. Chem. Lett. 6, 812–816 (2015).
- Cox, J. M. et al. Solvent exchange in a metal-organic framework single crystal monitored by dynamic in situ X-ray diffraction. *Acta Crystallogr. B* 73, 669–674 (2017).
- Cox, J. M., Walton, I. M., Benson, C. A., Chen, Y.-S. & Benedict, J. B. A versatile environmental control cell for in situ guest exchange single-crystal diffraction. J. Appl. Crystallogr. 48, 578–581 (2015).

NATURE CHEMISTRY ARTICLES

- 34. Yakovenko, A. A. et al. Study of guest molecules in metal–organic frameworks by powder X-ray diffraction: analysis of difference envelope density. *Cryst. Growth Des.* 14, 5397–5407 (2014).
- Chen, Y.-P., Liu, Y., Liu, D., Bosch, M. & Zhou, H.-C. Direct measurement of adsorbed gas redistribution in metal-organic frameworks. J. Am. Chem. Soc. 137, 2919–2930 (2015).
- Tan, J. C. & Cheetham, A. K. Mechanical properties of hybrid inorganicorganic framework materials: establishing fundamental structure-property relationships. *Chem. Soc. Rev.* 40, 1059–1080 (2011).
- Burtch, N. C., Heinen, J., Bennett, T. D., Dubbeldam, D. & Allendorf, M. D. Mechanical properties in metal-organic frameworks: emerging opportunities and challenges for device functionality and technological applications. *Adv. Mater.* 30, 1704124 (2018).
- Petkov, P. S. et al. Conformational isomerism controls collective flexibility in metal-organic framework DUT-8 (Ni). *Phys. Chem. Chem. Phys.* 21, 674–680 (2019).
- Chupas, P. J. et al. A versatile sample-environment cell for non-ambient X-ray scattering experiments. Appl. Crystallogr. 41, 822–824 (2008).
- Toby, B. H. & Von Dreele, R. B. GSAS-II: the genesis of a modern opensource all purpose crystallography software package. *J. Appl. Crystallogr.* 46, 544–549 (2013).
- Dubbeldam, D., Calero, S., Ellis, D. E. & Snurr, R. Q. RASPA: molecular simulation software for adsorption and diffusion in flexible nanoporous materials. *Mol. Simul.* 42, 81–101 (2016).
- 42. Burtch, N. C., Dubbeldam, D. & Walton, K. S. Investigating water and framework dynamics in pillared MOFs. *Mol. Simul.* 41, 1379–1387 (2015).
- Gaillac, R., Pullumbi, P. & Coudert, F.-X. ELATE: an open-source online application for analysis and visualization of elastic tensors. *J. Phys. Condens. Matter* 28, 275201 (2016).
- Kresse, G. & Hafner, J. Ab initio molecular dynamics for liquid metals. *Phys. Rev. B* 47, 558–561 (1993).

Acknowledgements

This work was supported as a part of the Center for Understanding and Control of Acid Gas-Induced Evolution of Materials for Energy, an Energy Frontier Research Center funded by the US Department of Energy, Office of Science, Basic Energy Sciences under award no. DE-SC0012577. Use of the Advanced Photon Source was supported by the US

Department of Energy, Office of Science, Office of Basic Energy Sciences, under contract no. DE-AC02-06CH11357. N.C.B. acknowledges support from the National Science Foundation Graduate Research Fellowship and the Graduate Research Opportunities Worldwide (GROW) award under grant no. DGE-1148903. D.D. acknowledges support from the Netherlands Research Council for Chemical Sciences through a VIDI grant and the Dutch Research Council (NWO) Exacte Wetenschappen (Physical Sciences) for the use of supercomputer facilities with financial support from the NWO. NSF's ChemMatCARS Sector 15 is supported by the Divisions of Chemistry (CHE) and Materials Research (DMR), National Science Foundation, under grant no. NSF/CHE-1834750. Use of the Advanced Photon Source, an Office of Science User Facility operated for the US Department of Energy Office of Science by Argonne National Laboratory, was supported by the US Department of Energy under contract no. DE-AC02-06CH11357.

Author contributions

All authors contributed extensively to the work presented in this paper. N.C.B., C.R.M., Y.J. and J.T.H. performed the powder synthesis and adsorption characterization work, and C.R.M. led the synchrotron diffraction analysis with help from N.C.B., A.A.Y. and W.X. The computational studies were performed by N.C.B., J.H. and D.D. SCXRD experiments and analysis were led by I.M.W. with assistance from Y.-S.C. and J.T.H. IR spectroscopy experiments and analysis were performed by J.T.H. and I.M.W. The manuscript was written by N.C.B., I.M.W and K.S.W. with input from the other authors.

Competing interests

The authors declare no competing interests.

Additional information

Supplementary information is available for this paper at https://doi.org/10.1038/s41557-019-0374-y.

Correspondence and requests for materials should be addressed to K.S.W.

Reprints and permissions information is available at www.nature.com/reprints.

Publisher's note Springer Nature remains neutral with regard to jurisdictional claims in published maps and institutional affiliations.

© The Author(s), under exclusive licence to Springer Nature Limited 2019